Journal of Catalysis 266 (2009) 79–91

Contents lists available at ScienceDirect

Journal of Catalysis

journal homepage: www.elsevier.com/locate/jcat

The role of the zeolite channel architecture and acidity on the activity and selectivity in aromatic transformations: The effect of zeolite cages in SSZ-35 zeolite

Naděžda Žilková [a], Martina Bejblová [a], Barbara Gil [b], Stacey I. Zones [c], Allen W. Burton [c], Cong-Yan Chen [c], Zuzana Musilová-Pavlačková [a], Gabriela Košová [a], Jiří Čejka [a,*]

[a] J. Heyrovský Institute of Physical Chemistry, Academy of Sciences of the Czech Republic v.v.i., Dolejškova 3, CZ-182 23 Prague 8, Czech Republic
[b] Department of Chemistry, Jagiellonian University, Ingardena 3, PL-30 060 Krakow, Poland
[c] Chevron Energy and Technology Company, Richmond, CA 94 802, USA

ARTICLE INFO

Article history:
Received 1 August 2008
Revised 16 May 2009
Accepted 20 May 2009
Available online 2 July 2009

Keywords:
Zeolite architecture
Cage effect
Acidity
Alkylation
Disproportionation
SSZ-33
SSZ-35
MCM-58
MCM-68

ABSTRACT

A series of zeolites differing in the channel architecture and acidity was investigated in toluene disproportionation, together with toluene and *p*-xylene alkylation with isopropyl alcohol. Zeolites with one- to three-dimensional 10-ring and 12-ring channels with and without cages, and those having 12–12–10 and 12–10–10-ring channel systems were studied. It was shown that general relationship of increasing zeolite activity with increasing pore diameter and pore connectivity is not valid as the size of some 12-ring channels (Beta, MCM-68) is comparable with 10-ring channels (ZSM-5, SSZ-35). In addition, the presence of cages in the structure of SSZ-35 and MCM-58 attributes the unusual catalytic behavior of these zeolites. SSZ-35 and MCM-58 zeolites behave in both toluene reactions such as three-dimensional large-pore zeolites. Subtle differences between zeolites of similar pore sizes and dimensionality can be usually explained based on the differences in the acidity of the individual zeolites. In *p*-xylene alkylation SSZ-35 exhibited high conversion with the highest selectivity to 1-isopropyl-2,5-dimethyl benzene and a low rate of deactivation. The presence of 18-ring cages in the channels of 10-ring zeolite SSZ-35 (STF) gives rise to an unusual catalytic behavior of this zeolite by comparison to other 10-ring zeolites. SSZ-35, possessing channels of 0.54×0.57 nm in diameter, exhibits catalytic activity in transformation of aromatic hydrocarbons that is similar to large-pore zeolites. 18-Ring cages enable the formation of relatively bulkier transition states while the diffusion of the product molecules out of the 10-ring channel system is not slowed down due to 10-ring windows. In addition, the channel system of SSZ-35 prevents the formation of coke precursors.

1. Introduction

More than 180 different structural types of zeolites were already recognized by the International Zeolite Association. The individual types of zeolites differ in the size of the channels (8-, 10-, 12-, 14-, or even larger rings), connectivity of the channels, and the presence or absence of cages in channel intersections or along the channel itself [1]. In addition to zeolite acidity, the size of channels and their dimensionality influence the activity and selectivity in transformations of organic compounds [2–4]. Reactions of alkyl and dialkyl aromatic hydrocarbons represent an interesting group of reactions both from the practical petrochemical viewpoint as well as model reactions usually influenced by shape selectivity [5,6]. Zeolites with 10 rings usually exhibit *restricted transition-state* and *product shape* selectivity being particularly important in *para*-selective reactions such as toluene disproportionation, xylene isomerization, and toluene alkylation with methanol, ethylene/ethanol, and propylene/propanol [7–14]. Diffusion coefficients of individual *ortho*, *meta*, and *para* isomers differ in several orders of magnitude, which completely changes the product mixture composition in comparison with conventional non-microporous catalysts [15].

The crystal size of zeolites is expected to substantially influence the conversion of aromatic hydrocarbons as well as the resulting selectivity, especially when related to the *para*-selectivity [16–19]. Unfortunately, most of the papers published show these selectivities for different conversions, which makes it impossible to provide clear conclusions. In this respect, Melson and Schűth showed, for ethylbenzene disproportionation, that external acidity plays a very important role due to the enrichment of aluminum in the crystal rim. Thus, the external acidity of zeolites increases substantially when decreasing the size of the crystals [18].

Zeolites represent the most important inorganic materials for catalysis, finding applications in dozens of technological processes from petroleum refining and petrochemistry up to fine chemical

* Corresponding author.
E-mail address: jiri.cejka@jh-inst.cas.cz (J. Čejka).

0021-9517/$ - see front matter © 2009 Elsevier Inc. All rights reserved.
doi:10.1016/j.jcat.2009.05.017

synthesis [5,9]. The synergism in zeolite synthesis and prediction of new zeolite structures increase the opportunities for their further application and deepen our knowledge on their behavior in catalytic reactions [20,21]. For a long time it was believed that zeolite activity increases mainly with increasing channel dimensions and connectivity of the channels. A typical example of this relationship is represented by the so-called Constraint Index, a test presented in a paper by Frillette et al. [22]. The Constraint Index relates the activity and selectivity of a zeolite to the ratio of the cracking rates of *n*-hexane to 3-methylpentane under standard reaction conditions. Various researchers have attempted to rationalize this relationship using this and other test reactions [23]. Novel zeolites with previously unknown structural features frequently show unexpected catalytic behavior. On the other hand, these 'standard' catalytic reactions can be used to characterize the internal pore architecture of unknown zeolites [24].

In a similar way, reactant conversions usually increase with the concentration of active sites while in some reactions the selectivity can be deteriorated by the presence of a high concentration of Lewis acid sites [5].

To differentiate the catalytic behavior of zeolites we investigated a series of different structural types of zeolites. Medium pore zeolites are represented by ZSM-5 (3-D channel structure with 10-ring channels) and SSZ-35 (1-D structure with 10-ring channels and 18-ring cages [25]). Typical large pore zeolites studied are Mordenite (1-D structure), MCM-58 (isostructural with ITQ-4 and SSZ-42 with undulating 1-D 12-ring system with cages [26]), and zeolite Beta (3-D 12-ring channel system). MCM-68 (3-D 12–10–10-ring channel system [27]) and SSZ-33 (3-D 12–12–10-ring system [28]) are examples of zeolites combining large and medium pore channels. Our knowledge on the catalytic behavior of zeolites with different structural types can provide a deeper insight when studying zeolites with yet unknown structures. It was already predicted for the, at that time unknown, structures of IM-5 and SSZ-57 [24]. In this case, catalytic results were combined with adsorption studies using 2,2-dimethylbutane as a probe molecule [29].

Finding the relationship among zeolite channel architecture, zeolite acidity, and activity and selectivity in toluene disproportionation as well as toluene and *p*-xylene alkylation with isopropyl alcohol is the main objective of this investigation. This relationship is influenced by two types of factors: (i) those associated to parameters of catalytic reaction (reaction temperature, space velocity, concentration of reactants, and thermodynamic equilibrium), and (ii) those related to the properties of the catalysts used (crystal size, channel size, and dimensionality of the channel system, type and strength of acid sites and their density and coking). While factors ad (i) were maintained constant during all measurements, we tried to analyze in more detail variables ad (ii) thus, those depending on the zeolites themselves. These include Si/Al ratio, concentration of Brønsted and Lewis sites, and their density as well as crystal size, because those are factors that cannot be adjusted completely in the same way for all zeolites under study. On the other hand, detailed analysis of acidic properties of zeolites under study provides us with a nice opportunity to correlate the catalytic behavior of these zeolites and their structural features.

Toluene disproportionation was chosen as one of these reactions because it reflects not only the structural features and acidity of the zeolite catalysts under study, due to the possibility of monomolecular and bimolecular mechanism, but also the product selectivity for preferential xylene formation [5,30,31]. Toluene alkylation provides even more information about the reaction volume and acidity of zeolites due to the parallel alkylation/disproportionation reactions, selectivity to cymenes/*p*-cymene, and also a possible formation of secondary products such as *n*-propyl toluene requiring a particular channel arrangement [32,33]. As for the *p*-xylene alkylation, the product of the first alkylation step is always 1-isopropyl-2,5-dimethyl benzene and all other products can be formed via secondary reactions. The details of their channel systems are provided in Table 1. In addition, this contribution evidences the importance of 18-ring cages in the 1-D 10-ring channel system of zeolite SSZ-35. This zeolite exhibits higher reaction rates than those for other three-dimensional 10-ring or even large-pore zeolites. SSZ-35 has a system of 1-D 10-ring channels that periodically open into wide, shallow cavities that are circumscribed by an 18-ring (Fig. 1) [25]. Only a few zeolites with such interesting structures have been described up-to-date in the literature [34], but the effect of their cages on the catalytic behavior has not yet been reported.

Table 1
Structural features of zeolites under study. Reference samples are marked with asterisks.

Zeolite	IZA code	Channel dimensionality	Channel entrances	Channel diameter (nm)
MOR*	MOR	2-D	12–8	0.65 × 0.70 0.26 × 0.57
BEA*	BEA	3-D	12–12–12	0.66 × 0.76 0.56 × 0.56
ZSM-5*	MFI	3-D	10–10–10	0.53 × 0.56 0.51 × 0.55
MCM-58	IFR	1-D	12	0.62 × 0.72
MCM-68	MSE	3-D	12–10–10	0.64 × 0.68 0.52 × 0.58 0.52 × 0.52
SSZ-33	CON	3-D	12–12–10	0.64 × 0.70 0.70 × 0.59 0.51 × 0.45
SSZ-35	STF	1-D	10	0.54 × 0.57

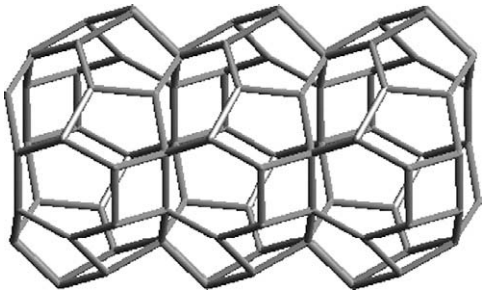

Fig. 1. View of 3 STF cages that stack to form the 1-dimensional pore in SSZ-35.

2. Experimental

2.1. Catalysts under study

Synthesis, properties and characterization of all zeolites under study were already reported, e.g. SSZ-33 and SSZ-35 [35,36], Beta and Mordenite [37], and MCM-58 and MCM-68 [38]. As an essential interest has been paid here to SSZ-35, its synthesis is briefly discussed. The SSZ-35 zeolite was prepared according to Ref. [39]. The synthesis of SSZ-35 itself was carried out in a 4-l reactor containing a Hastelloy C liner. Into the liner 0.45 mol of the SDA in 727 g of water (plus additional 950 g) was introduced. Then 300 g of 1 M KOH solution was added. Reheis F2000 (hydrated aluminum hydroxide containing 50–53 wt% Al_2O_3) was used as a source of aluminum. 7.31 g (37 mmol) of it was added to the reaction mixture and finally 185 g of Cab–O–Sil M5 (97% SiO_2, Cabot) was introduced to give 3 mol of SiO_2. The reaction was seeded at the 0.9 wt% level. The resultant mixture was heated to 160 °C (15 °C/min ramp up), and stirred at 150 rpm for 2.5 days. The synthesized SSZ-35

was calcined in an oven with a stream of nitrogen gas passing over the zeolite in thin coverage on trays. The program was run at 1 °C/min to 120 °C, maintained at 120 °C for 2 h, then heated (1 °C/min) to 540 °C, kept for 5 h, and further heated to 595 °C (1 °C/min), and maintained for another 5 h.

All zeolites were transformed to ammonium forms via four-time repeated ion-exchange using 0.5 M aqueous solution of ammonium nitrate at ambient temperature for 5 h. The only exception is SSZ-33, originally prepared as boron form. After the replacement of boron for aluminum the protonic form was obtained directly [40].

2.2. Characterization of catalysts

The crystallinity of zeolites was determined by X-ray powder diffraction with a Bruker D8 Advance X-ray powder diffractometer equipped with a graphite monochromator and position-sensitive detector using CuKα radiation in Bragg–Brentano geometry. Diffractograms of all zeolites used exhibit a good crystallinity and characteristic diffraction lines for these materials. No additional crystalline phases were observed in the diffraction patterns.

The shape and size of zeolite crystals were determined by scanning electron microscopy (Jeol, JSM-5500LV). Also SEM images evidence the absence of impurities including an amorphous one. As the crystal size is of a high importance for the present comparison study, we carefully chose zeolites with crystal sizes between 0.3 and 1 μm. The composition of synthesized zeolites was determined on a Philips PW 1404 X-ray fluorescence spectrometer. Calcined samples were homogenized using agate mortar and after adding of dentacryle as a binder they were deposited on a surface of cellulose tablets.

2.3. Catalytic reactions

Toluene disproportionation and alkylation with isopropyl alcohol were investigated in the gas phase under atmospheric pressure using a glass fixed-bed microreactor. Each catalyst was pressed into the pellets, crushed and sieved to obtain particles with a diameter in the range of 0.50–0.71 mm. Prior to the reaction, a given amount of the catalyst was *in situ* activated at 500 °C for 120 min in a stream of nitrogen (40 ml min^{-1}), and then the activated catalyst was cooled down to the preset reaction temperature. In the case of toluene disproportionation the reaction temperature was at 450 and 500 °C, WHSV 2 and 20 h^{-1}, and the concentration of toluene in a stream was 18.5 mol%. Toluene alkylation was studied at the reaction temperatures 200 and 250 °C. The WHSV related to toluene was 10 h^{-1}, the concentration of toluene was 18.5 mol%, and toluene to isopropyl alcohol molar ratio was 9.6.

The reaction mixtures were analyzed using an *on-line* gas chromatograph (HP 6890) equipped with an FID detector and a capillary column (DB-5, 50 m × 320 μm × 1 μm) in toluene alkylation, while HP-INNOWax column (30m × 0.32 mm × 0.5 μm) was used for toluene disproportionation studies. The first sample was taken after 15 min of time-on-stream (T-O-S) and the other samples were taken in the interval of 60 min.

The alkylation of *p*-xylene with isopropyl alcohol was performed in a down-flow glass microreactor with a fixed bed of catalyst under atmospheric pressure. Zeolite powder was pressed into the pellets, crushed, and sieved to obtain particles between 0.50 and 0.71 mm. Prior to the reaction, 0.4 g of catalyst was activated at 450 °C in 40 ml/min of nitrogen for 120 min and then cooled to the reaction temperature of 150 °C. All experiments were carried out under 0.2 h^{-1} WHSV based on *p*-xylene (SSZ-35, SSZ-33, ZSM-5) or 0.5 h^{-1} (Beta) with *p*-xylene to isopropyl alcohol molar ratio of 0.5. The reaction products were analyzed using an on-line gas chromatograph (HP 5890A) equipped with an FID detector and a Supelcowax 10 capillary column (30 m long). The first analysis was performed after 15 min of time-on-stream and the others followed with the interval of 44 min.

2.4. Infrared measurements

The acidity of zeolites was investigated by adsorption of pyridine and pivalonitrile (*tert*-butyl cyanide, $(CH_3)_3CCN$) used as probe molecules followed by FTIR spectroscopy. All samples were activated in a form of self-supporting wafers (ca 5 mg/cm^2) at 550 °C under vacuum for 1 h prior to the adsorption of probe molecules. The adsorption temperatures were: pyridine (POCh Gliwice, analytical grade, dried over 3A molecular sieve) at 170 °C and pivalonitrile (Aldrich, 99%) at ambient temperature. Spectra were recorded on a Bruker Tensor 27 spectrometer with a resolution of 2 cm^{-1} and an MCT detector. All measured spectra were recalculated to a 'normalized' wafer of 10 mg. For a quantitative characterization of acid sites the following bands and absorption coefficients were used: pyridine PyH^+ band at 1545 cm^{-1}, ε = 0.078 cm μmol^{-1} pyridine PyL band at 1454 cm^{-1}, ε = 0.165 cm μmol^{-1} [41].

2.5. Molecular modelling

Calculations were performed with the Cerius2 [42] software using a combination of the Burchart [43] and Universal forcefields [44] to evaluate the van der Waals interactions of the organic molecules within the zeolite framework. We model each zeolite structure as an all-silica framework.

3. Results and discussion

Dialkylbenzenes are not only important raw materials in the chemical industry but also their formation provides important knowledge on the structure and acidity of zeolite catalysts. For both toluene disproportionation and its alkylation with isopropyl alcohol over ZSM-5 zeolite, the formation of *para*-isomers can be expected to proceed almost exclusively in the zeolite channel system, while the formation of *meta*- and *ortho*-isomers proceeds on the external surface [45]. Increasing conversion leads to the decrease in *para*-selectivity for ZSM-5 enhancing the rate of subsequent reactions. The same effect can be seen for decreasing the size of zeolite crystals. It was pointed out by Melson and Schűth in ethylbenzene disproportionation [18] that small ZSM-5 crystals possess a high concentration of acid sites on their external surface. As a result, consecutive isomerization reaction proceeds with a higher rate decreasing the desired selectivity to *para*-isomer in favor of *meta*- and *ortho*-diethylbenzenes. The increase in the size of channels from medium- to large-pore zeolites causes the increase in the toluene conversion while selectivities to para-dialkylbenzenes are close to thermodynamic values [46]. Thus, when only geometric factor would be considered the conversions of toluene and *p*-xylene in reactions investigated should increase in the sequence SSZ-35 < ZSM-5 < MCM-58 ~ Mordenite < MCM-68 < SSZ-33 < Beta, following the dimensionality and channel sizes. However, it has to be mentioned that a 12-ring channel of zeolite Beta is close in size to 10-ring channels (Table 1). In addition to that, the presence of cages in SSZ-35 and MCM-58 influences the conversion as well. Last but not least we have to consider the effect of acidity – type, concentration, and strength of acid sites.

3.1. Acidity study: concentration and strength of the acid sites

The acidity of zeolites MCM-58, MCM-68, SSZ-33, and SSZ-35 as well as reference samples (Beta, Mordenite and ZSM-5) was

Table 2
Acid properties of zeolites studied in this work. The number of Brønsted and Lewis acid sites from elemental analysis and IR studies of pyridine sorption. PyH^+ – Brønsted sites (from the intensity of 1545 cm^{-1} band), PyL – Lewis sites (1454 cm^{-1} band). The values PyH^+ (520/170) and PyL (520/170) represent a fraction of pyridine still bonded onto Brønsted or Lewis sites after desorption at 520 °C with respect to the total number of acidic centers.

Zeolite	XFS			Pyridine des. temp. (°C)	IR		IR acid strength	
	Si/Al	Al per u.c.	Al mmol/g		PyH^+ mmol/g	PyL mmol/g	PyH^+ 520/170	PyL 520/170
MOR	9.5	4.60	1.595	170	1.416	0.018		
				520	0.398	0.031	0.28	1.72
BEA	12.5	4.70	1.222	170	0.343	0.432		
				520	0.030	0.279	0.09	0.65
ZSM-5	34.5	2.70	0.468	170	0.220	0.046		
				520	0.072	0.022	0.33	0.48
MCM-58	36	0.86	0.447	170	0.496	0.035		
				520	0.213	0.068	0.43	1.94
MCM-68	13	8.00	1.184	170	0.635	0.113		
				520	0.239	0.111	0.38	0.98
SSZ-33	18	2.90	0.875	170	0.299	0.428		
				520	0.178	0.302	0.60	0.71
SSZ-35	38.5	0.40	0.416	170	0.260	0.042		
				520	0.114	0.052	0.44	1.24

investigated by pyridine adsorption. Pyridine of kinetic diameter 0.5 nm was able to react with all acidic hydroxyl groups in all zeolites studied here with an exception of Mordenite, for which hydroxyl groups localized in 8-ring channels (0.26×0.57 nm) were inaccessible for steric reasons. Nevertheless, these sites in Mordenite were not accessible for toluene as well. So the acidity measured in this manner is more adequate to the actual catalytic capability of this zeolite, as tested by toluene reactions. Pyridine was adsorbed in excess at 170 °C and then desorbed at the same temperature for 20 min to remove the gas phase and weakly bonded species. The intensity of the IR bands of protonated and coordinatively bonded pyridine, together with respective absorption coefficient, were used to determine the concentration of Brønsted and Lewis sites. Calculated concentrations are presented in Table 2. Individual zeolites under study differ in Si/Al ratio as well as in the concentrations of Brønsted and Lewis acid sites. The order of the concentrations of Brønsted acid sites, calculated for 1g of activated zeolite, is ZSM-5 < SSZ-35 < SSZ-33 < Beta < MCM-58 < MCM-68 < Mordenite. If the total amount of acid sites (Brønsted plus Lewis) is taken into account, the order is slightly different: ZSM-5 < SSZ-35 < MCM-58 < SSZ-33 < MCM-68 < Beta < Mordenite, mainly because of the high concentration of Lewis sites in zeolites Beta and SSZ-33.

There are two methods for studying the acid strength of OH groups in zeolites. The first one is thermodesorption of a strong base, such as ammonia or pyridine (a dynamic experiment). The second one is adsorption of a weak base, such as CO, and comparison of the value of the red-shift of the OH groups in the IR spectrum, which is caused by the interaction with the adsorbate (static experiment). Thermodesorption is more suitable for testing the acidity being further compared with the test reactions because, besides the intrinsic acidity, it can also test (to some extend) the diffusion restrictions in the channels. Acid strength is visualized here as the percent of pyridine still present in the zeolite after desorption at 520 °C with the intensity of the pyridine bands after desorption at 170 °C taken as 100%. The higher the percentage of the pyridine kept after desorption at 520 °C, the stronger the acid centers of the zeolite. The acid strength of the Brønsted centers (value $PyH^+_{520/170}$ in Table 2) is in the order: Beta < Mordenite < ZSM-5 < MCM-68 < MCM-58 < SSZ-35 <SSZ-33. It is worth to note that for most of the zeolites, Lewis acid sites are much stronger than the Brønsted acid sites. With zeolites such as MCM-58, SSZ-35, and Mordenite, the intensity of the band characteristic of coordinatively bonded pyridine was even higher after desorption at higher temperatures, resulting in $PyL_{520/170}$ values higher than 1. The increase in the intensity of the band of pyridine bonded onto Lewis sites during thermodesorption can be caused by either the increased accessibility of some sites at high temperature (Mordenite) or by the appearance of the second band of coordinatively bonded pyridine as reported by us for SSZ-35 [47]. For toluene disproportionation carried out at 450 and 500 °C a high concentration of Lewis sites can promote the inductive influence of Lewis acid sites on the acid strength of the neighboring Brønsted centre [48].

3.2. Acidity studies: accessibility and diffusivity

Pyridine is so basic molecule that it is able to withdraw protons from their positions attached to the framework. Therefore, to assess the differences in accessibility of all the acid sites in zeolites with 10- and 12-rings, pivalonitrile (*tert*-butyl cyanide) was chosen as another probe molecule. It was already proved that the 10–10-ring system of ZSM-5 is completely inaccessible for pivalonitrile [49] and novel zeolites are investigated here: MCM-68 (12–12–10-ring), SSZ-33 (12–10–10-ring), and SSZ-35 (10-ring portals with opening to 18-ring cavity) are composed of such channels (Fig. 2). Unfortunately, it cannot be generalized that pivalonitrile cannot enter any of 10-ring channels as we have recently shown that all Brønsted type sites are available for pivalonitrile in SSZ-33 and even in SSZ-35 [47]. The comparison of acid site concentration in individual zeolites, together with their acid strength related to pyridine and pivalonitrile, is presented in Fig. 3. For ZSM-5 zeolite used in this work, some OH groups are consumed after pivalonitrile introduction at room temperature, which indicates that this particular sample can contain some mesopores providing an access to the channels of this zeolite. Other zeolites are composed of 12-rings and therefore should be entirely open to pivalonitrile although the size of one of the channels in both SSZ-33 and Beta is rather close to 10-ring channels (Table 1). Fig. 2A–C show that all OH groups are consumed when pivalonitrile is adsorbed in MCM-68, MCM-58, SSZ-33, SSZ-35, and Beta. Similar to pyridine, pivalonitrile was also desorbed at increasing temperatures to show, whether the bulkier molecule (kinetic diameter 0.6 nm) with its three methyl groups makes it much stiffer than flat pyridine, whether the diffusion inside different channels will be more diverse. The intensity of the band at 1374 cm^{-1} (CH_3 umbrella bending of pivalonitrile) was taken as the analytical band, representing the amount of pivalonitrile still kept in zeolite after desorption at 250 °C. The differences between zeolites are a little bit larger for desorption of pivalonitrile than for that of pyridine (Fig. 3). The order, in which zeolites release pivalonitrile, is slightly different from the order in which pyridine was desorbed. It reflects

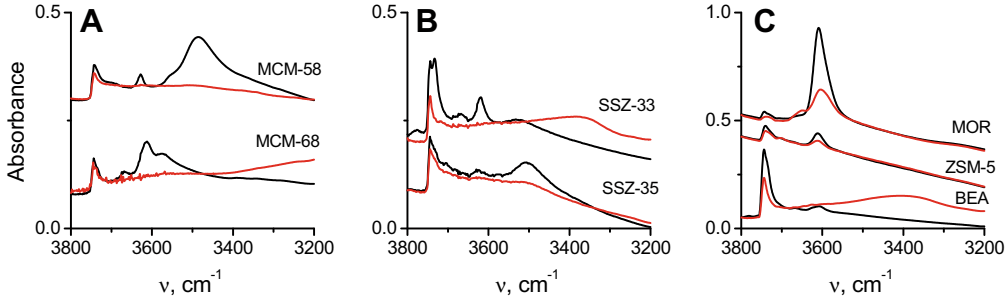

Fig. 2. IR spectra in the OH region of studied zeolites before (black lines) and after (red lines) pivalonitrile sorption at RT and consecutive 20 min desorption at RT. (For interpretation of the references to colour in this figure legend, the reader is referred to the web version of this article.)

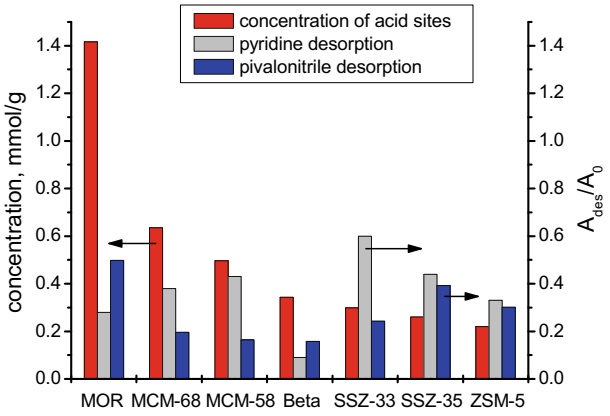

Fig. 3. Concentration and the strength of Brønsted acid sites. Red bars represent concentration of Brønsted centers (mmol/g) measured by pyridine sorption. Gray bars represent the strength of Brønsted centers: the value A_{des}/A_0 is the ratio of the intensities of PyH^+ band after pyridine desorption at 170 °C (A_0) and 520 °C (A_{des}). Blue graphs represent the ease of desorption for pivalonitrile: the value A_{des}/A_0 is the ratio of the intensities of pivalonitrile's CH_3 bending band after pivalonitrile desorption at room temperature (A_0) and 250 °C (A_{des}). (For interpretation of the references to colour in this figure legend, the reader is referred to the web version of this article.)

the easier diffusion rather than the differences in acid strength because pivalonitrile molecule is only slightly basic and very rigid. The achieved order is Beta < MCM-58 < MCM-68 < SSZ-33 < ZSM-5 < SSZ-35 < Mordenite. What is surprising is the fact that Mordenite seems to be the least acidic when tested by pyridine desorption, when tested by pivalonitrile it is now the last in the order, strongly keeping pivalonitrile. Such behavior of Mordenite shows the best that when it comes to reactions of molecules of diameter close to the channel diameter, the type of channels, their size, and connectivity can alter the reaction course. The comparison of acid site concentration in individual zeolites, together with their acid strength related to pyridine and pivalonitrile is provided in Fig. 3.

3.3. Catalytic investigations

The catalytic activity of zeolites MCM-68 (12–12–10), SSZ-33 (12–10–10), Beta (12–12–12), Mordenite (12–8), MCM-58 (undulating 12-ring), SSZ-35 (10-ring portals with opening to 18-ring cavity), and ZSM-5 (10–10–10) was investigated in toluene disproportionation as well as toluene and *p*-xylene alkylation with isopropyl alcohol. The crystals size of SSZ-33 and Beta is about 0.2–0.3 μm, MCM-68 exhibits crystals around 0.5 μm while crystals of ZSM-5 and SSZ-35 are a little bit larger being around 1 μm. Only MCM-58 possesses crystals being around 3–5 μm, however, even such a large size of the crystals did not lead to a substantial decrease in toluene conversion or fast deactivation. Thus, the size of all crystals provides a nice opportunity to compare the catalytic behavior of zeolites in toluene or *p*-xylene transformations. However, it should be pointed out that even when the same crystal sizes of 1-D and 3-D channel systems of zeolites are used the accessibility of their channels has to be very different.

X-ray powder diffraction and scanning electron images (not given here, for details see Refs. [35–38]) provide clear evidence about the high-quality and phase purity of these materials. Nitrogen and argon adsorption measurements were used to determine the micropore volume, which shows the openness of the structure without amorphous species blocking the access to the channel system.

3.4. Toluene disproportionation

The toluene conversions (at 60 min of T-O-S) in toluene disproportionation carried out at 450 and 500 °C follow the order ZSM-5 < Mordenite ≈ Beta < SSZ-35 < MCM-68 < MCM-58 < SSZ-33 and ZSM-5 < Beta < SSZ-35 ≈ MCM-68 < SSZ-33 ≈ MCM-58 < Mordenite, respectively (see Fig. 4A and B). From the comparison of toluene conversions at reaction temperatures of 450 and 500 °C we obtained the order ZSM-5 < Beta < SSZ-35 < MCM-58 ⩽ SSZ-33, while a quick deactivation of Mordenite and MCM-68 shifts their positions depending on the reaction temperature and the progress of deactivation is higher for increased reaction temperature. Anyway, both orders of toluene conversion do not match either with the order of the concentrations of Brønsted acid sites, calculated for 1 g of activated zeolite (ZSM-5 < SSZ-35 < SSZ-33 < Beta < MCM-58 < MCM-68 < Mordenite), or with a total amount of acid (Brønsted plus Lewis) sites (ZSM-5 < SSZ-35 < MCM-58 < SSZ-33 < MCM-68 < Beta < Mordenite) calculated on the basis of IR measurements (cf. Tables 2 and 3). If acid sites would be considered as decisive for toluene conversion then MCM-68 and Mordenite should provide the highest toluene conversions. Actually, after 60 min of T-O-S the highest conversion was reached over Mordenite but MCM-68 exhibited comparable conversion with SSZ-35. At 450 °C the toluene conversion of Mordenite is even lower than, e.g. SSZ-33, MCM-58, MCM-68, and SSZ-35 (Fig. 4A). In addition, both Mordenite and MCM-68 deactivated very quickly compared with other zeolites, most probably due to a high density of OH groups – in both cases ca. $4H^+$/u.c.

3.4.1. The effect of zeolite channel architecture

Toluene conversions do not follow the order of the channel sizes and their dimensionality. In such cases zeolite Beta followed by SSZ-33 and MCM-68 should dominate. While SSZ-33 provided at the reaction temperature of 500 °C the toluene conversion 56% after 60 min of T-O-S (only Mordenite was more active but quickly

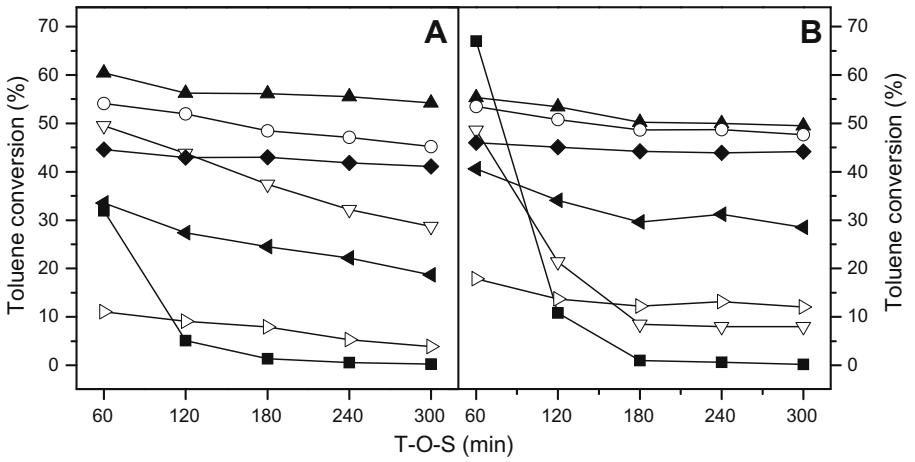

Fig. 4. T-O-S dependence of toluene conversion in toluene disproportionation over different structural types of zeolites (WHSV – 2.0 h^{-1}, reaction temperature 450 °C (A) and 500 °C (B); (◄) BEA, (▽) MCM-68, (▲) SSZ-33, (○) MCM-58, (■) MOR, (▷) ZSM-5, (♦) SSZ-35).

Table 3
The orders of zeolites with respect to the concentration and strength of acid sites, as well as conversion in disproportionation of toluene after 60 min T-O-S (at 500 °C) and alkylation of toluene with isopropyl alcohol after 15 min of T-O-S (at 250 °C).

Concentration of acid sites			Strength of acid sites			Toluene conversions	
Brønsted	Lewis	All	Brønsted	Lewis	All	Disprop.	Alkylation
Mordenite	Beta	Mordenite	SSZ-33	MCM-58	MCM-58	Mordenite	SSZ-33
MCM-68	SSZ-33	Beta	SSZ-35	Mordenite	Mordenite	SSZ-33	MCM-68
MCM-58	MCM-68	MCM-68	MCM-58	SSZ-35	SSZ-35	MCM-58	SSZ-35
Beta	ZSM-5	SSZ-33	MCM-68	MCM-68	MCM-68	MCM-68	Beta
SSZ-33	SSZ-35	MCM-58	ZSM-5	SSZ-33	SSZ-33	SSZ-35	MCM-58
SSZ-35	MCM-58	SSZ-35	Mordenite	Beta	ZSM-5	Beta	Mordenite
ZSM-5	Mordenite	ZSM-5	Beta	ZSM-5	Beta	ZSM-5	ZSM-5

deactivated), toluene conversion over zeolite Beta was just slightly higher than 40% and only ZSM-5 exhibited lower conversion. These results clearly show that the order of toluene conversions cannot be directly related to the increasing pore size or connectivity of individual zeolite channels. Otherwise SSZ-35 would exhibit a lower or comparable toluene conversion than with ZSM-5 and in the same way toluene conversion over zeolite Beta would be higher than or comparable with that over SSZ-33. The effect of crystal size can be ruled out particularly for ZSM-5 vs. SSZ-35 vs. MCM-68 (1 μm vs. 0.3 μm vs. 0.5 μm) and Beta vs. SSZ-33 (both 0.3 μm). While the concentrations of aluminum in the framework of ZSM-5 (Si/Al = 37.5) and SSZ-35 (Si/Al = 38.5) as well as the concentrations of Brønsted sites 0.22 mmol g^{-1} and 0.26 mmol g^{-1} are comparable, the differences in toluene conversion after 60 min T-O-S are considerable, 20.0% (ZSM-5) and 46.5% (SSZ-35).

The most active zeolite as for the toluene conversion after 60 min of T-O-S (Mordenite) deactivated very quickly and after 180 min of T-O-S toluene conversion was lower than 10%. The high density of acid sites is most probably the main reason for deactivating so fast while the dimensionality of the channel system is of lower importance. This deactivation is due to the formation of coke deposits. It was observed that within relatively short reaction times, the color of Mordenite turned from white to black. The rate of the deactivation for all other zeolites under study is much slower and after 180 min of T-O-S the highest conversions were reached over SSZ-33 (53%) > MCM-58 (52%) > SSZ-35 (47%). While this is not surprising for three-dimensional SSZ-33 having 12–12–10-ring channel system, in the case of MCM-58 (1-D and 12-ring) and SSZ-35 (1-D and 10-ring) lower conversions were expected. The results of this study are mainly controlled by two following factors, namely, chemical and structural ones:

(i) similar strength of Brønsted acid sites, recently established for SSZ-33 and SSZ-35 [51], but a higher concentration of strong Lewis acid sites in SSZ-33 could promote a higher rate of the disproportionation reaction (cf. Table 2).
(ii) periodically located cavities in the structure of MCM-58 and SSZ-35 enable faster transport of reactants and products even if the structure is in principle one-dimensional.

The toluene conversions in toluene disproportionation over zeolites with different channel sizes and architecture clearly evidence that there is no general and unambiguous relationship between the size of the pores and their channel dimensionality and conversions in individual reactions. This rationalization was attempted by Haag and his colleagues by the so-called Constraint Index (CI), catalytic test based on the comparison of the reaction rates for the cracking of *n*-hexane (*n*-C6) and its isomer 3-methylpentane (3-MP) under comparable conditions [22]. Detailed investigations of this concept with an increasing number and diversity of zeolite structures by Zones and Harris provided the evidence that there are several limitations, under which this concept is not valid [23]. One of obstacles observed concerns the catalytic behavior of medium-pore zeolites possessing larger cavities, which do not show medium-pore behavior in the CI test (e.g. SSZ-35). The presence of 18-ring cavities in the channel structure of SSZ-35 probably explains high toluene conversions in toluene disproportionation, a behavior comparable even with 3-D 12-ring zeolite Beta. Similarly, high toluene conversions were achieved over 1-D Mordenite as well as MCM-58 exhibiting cages of about 1 nm in its 12-ring undulating system of channels. These cages are formed around benzyl-*N*-quinuclidine being used as template for the synthesis of MCM-58 [26]. The cages are able to accommodate a

transition state in bimolecular reaction between toluene and isopropyl toluene leading to the formation of *n*-propyl toluene [50]. Toluene conversion over both zeolites is much higher than expected based on a channel size – conversion model (CI test).

Previous results also show that both toluene conversions and xylene selectivities cannot be directly related to the channel architecture of different zeolites. Our detailed investigation of acidic properties of zeolites under study provided an order of increasing concentration of Brønsted sites as follows: ZSM-5 < SSZ-35 < SSZ-33 < Beta < MCM-58 < MCM-68 < Mordenite (Table 3). When the number of all acid sites (Brønsted plus Lewis) is considered, the concentration of all acid sites has the following order: ZSM-5 < SSZ-35 < MCM-58 < SSZ-33 < MCM-68 < Beta < Mordenite. In contrast, the increasing order of toluene conversions after 60 min of T-O-S is ZSM-5 < Beta < SSZ-35 ≈ MCM-68 < SSZ-33 ≈ MCM-58 < Mordenite. Although coke formation results in the decrease in toluene conversion mainly for Mordenite and MCM-68, still the highest toluene conversion at 60 min of T-O-S at 500 °C was obtained over Mordenite, for which the number of acid sites was much higher than for other zeolites (two to even seven times). From the comparison of acid sites and toluene conversion orders it is clearly seen that particularly large-pore zeolites Beta and MCM-58 do not follow these orders. On the other hand, medium-pore zeolite SSZ-35, with almost the lowest amount of Brønsted acid sites and a 1-D 10-ring channel system, provides much higher toluene conversion than expected. This can be explained by the positive effect of the presence of the unique STF cages on the catalytic activity of this zeolite.

3.4.2. The effect of type and concentration of acid sites

To get a deeper insight in the understanding of the decisive effects of zeolite for toluene disproportionation, toluene conversion was investigated in relation to the strength of Brønsted acid sites and all acid sites (Table 3). In this case the following sequences were obtained: Beta < Mordenite < ZSM-5 < MCM-68 < MCM-58 < SSZ-35 < SSZ-33 for Brønsted sites and Beta < ZSM-5 < SSZ-33 < MCM-68 < SSZ-35 < Mordenite < MCM-58 for all sites. Neither of them can be related to the increasing toluene conversion in toluene disproportionation. Although the highest "acid strength" was obtained over MCM-58, MCM-68, SSZ-33, and SSZ-35, the highest toluene conversion was reached over Mordenite despite the fact that this zeolite possessed a relatively low concentration of very strong acid sites. In this case, however, the high concentration of Brønsted acid sites in Mordenite (six times higher than the concentration of Brønsted sites in ZSM-5 the zeolite showing the lowest activity in toluene disproportionation) can compensate for its relatively low acid strength.

The prolongation of the reaction time makes this correlation even more complex. The primary reason is that the higher is the acid strength of the acid sites and the larger is the zeolite void reaction volume, the faster is also the deactivation, which is clearly visible mainly for SSZ-33 and MCM-68. In contrast, 1-D SSZ-35 and MCM-58 exhibited some stability against coking.

3.4.3. Transition states in SSZ-35

From the mechanistic point of view, toluene disproportionation is a bimolecular reaction requiring a reasonable reaction volume for the formation of the bimolecular transition state. This bimolecular state was even proposed for xylene isomerization in ZSM-5, being formed in the channel intersections [51]. With respect to that, formation of this bimolecular transition state should be severely limited in the1-D channel system of medium-pore zeolites such as SSZ-35. In contrast, SSZ-35 with 1-D channels system exhibits substantially higher conversion than ZSM-5 zeolite. In this case, a specificity of the structure of SSZ-35 having 1-D 10-ring channel system periodically opened into wide shallow cavities with 18-ring openings should be considered. One can infer that high toluene conversion in SSZ-35 is due to the presence of these 18-ring cavities being larger than the ZSM-5 channel intersections. Then, the formation of bimolecular transition state is not sterically limited. Also the 10-ring portals of SSZ-35 with opening to 18-ring cages do not decrease considerably the diffusion of reactants and products as such structure displays some flexibility, especially at higher reaction temperatures, where molecules even bulkier than the channel apertures can easily enter the interior of channels.

Molecular modeling shows that diphenylmethane-like precursors of toluene disproportionation are suitably positioned inside the channels of SSZ-35, assuming some interplay of these precursors located in two adjacent cages with one toluene molecule in each of them. Fig. 5A shows examples of low-energy configurations found for toluene molecules in neighboring cages. Although these models are not the direct indicators of the transition states and their energies, they show that each cage of SSZ-35 confines a single aromatic molecule so that it is in a likely position to disproportionate with another molecule in an adjacent cage. These configurations are therefore the probable precursors to

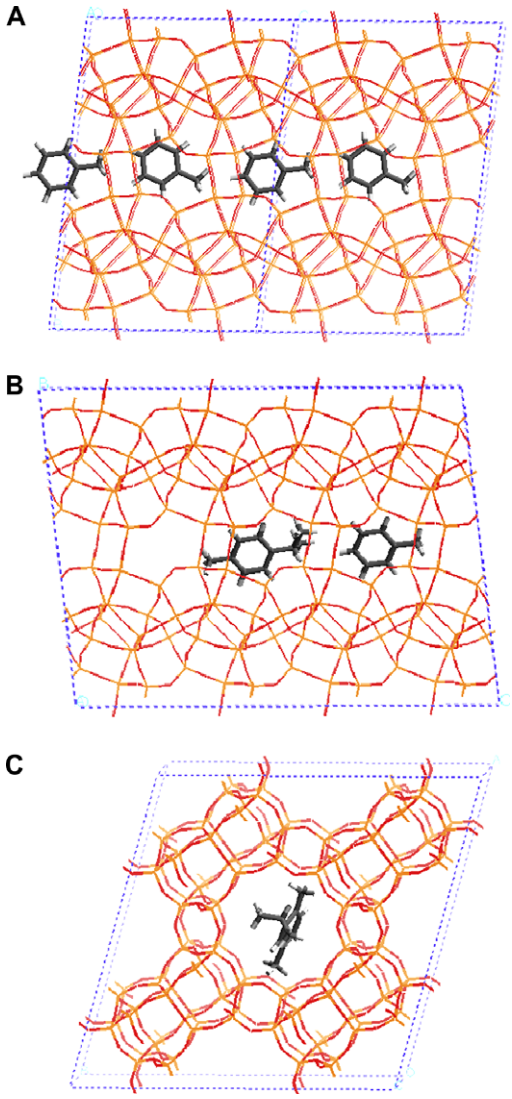

Fig. 5. (A) Possible configuration of toluene molecules preceding disproportionation transition state. (B) Possible configuration of cymene/toluene molecules in SSZ-35 preceding disproportionation transition state. (C) Configuration for 1-isopropyl-2,5-dimethylbenzene in SSZ-35 cavity with energy of −29.9 kcal/mol relative to gas phase molecule.

the transition state for toluene disproportionation. Note that the presence of more than one molecule per cage is unfavorable due to van der Waals repulsions between molecules within the same cage. It is also worth to note that the configurations shown in Fig. 5A have approximately co-planar aromatic rings as is expected for the disproportionation transition state. The methyl group, being transferred from one toluene molecule to another is located close to the 10-rings while the location of the second methyl group seems to be incidental as the energies of the related configurations for methyl group parallel or perpendicular to the channel axes are practically the same.

3.4.4. Selectivity to benzene and xylenes

In the ideal case of toluene disproportionation, benzene and xylenes are the products of the reaction of two toluene molecules, which should result in xylenes/benzene molar ratio equal to 1. Xylenes/benzene molar ratios after 60 min of T-O-S were found in the order SSZ-33 < MCM-58 ≈ MCM-68 < Mordenite < Beta < SSZ-35 < ZSM-5 (Fig. 6). This order although measured at different toluene conversion values reflects the decreasing reaction volume provided by individual zeolites. At the reaction temperature of 500 °C the highest values of xylene/benzene molar ratio achieved were 0.85-0.90 for zeolite ZSM-5, depending on T-O-S. For all other zeolites xylene/benzene ratios were much lower (0.40–0.70 at 60 min of T-O-S). It indicates that while the bimolecular transition state required for toluene disproportionation can be formed in the ZSM-5 channel system, the formation of more bulky transition states is limited due to the steric restrictions. With SSZ-35 the 18-ring cages play a particular role in subsequent reactions decreasing xylene/benzene ratio to 0.7 with a slight increase with T-O-S. Xylene/benzene ratios over Mordenite, MCM-58, and MCM-68 are even lower being close to 0.6 after 60 min of T-O-S. This reflects even larger free reaction space inside of these zeolites. MCM-58 and MCM-68 exhibited a high increase in xylenes/benzene molar ratio with T-O-S, which in a similar way to SSZ-33 confirms the formation of a large amount of coke deposits. It is expected that coke deposits decrease the reaction void volume and thus limit the consecutive reactions decreasing the selectivity to xylenes.

Selectivity to the sum of xylene isomers after 60 min of T-O-S increases in the order (Mordenite < MCM-68 ∼ SSZ-33 < MCM-58 < Beta < SSZ-35 < ZSM-5), although different toluene conversions have to be considered (Fig. 7). The rate of the byproduct formation,

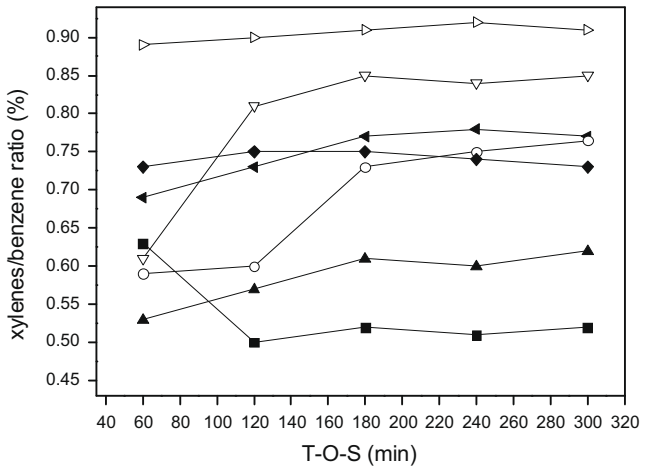

Fig. 6. T-O-S dependence of xylene to benzene molar ratio in toluene disproportionation over different structural types of zeolites (WHSV – 1.9 h^{-1}, reaction temperature 500 °C; (◄) BEA, (▽) MCM-68, (▲) SSZ-33, (○) MCM-58, (■) MOR, (▷) ZSM-5, (♦) SSZ-35).

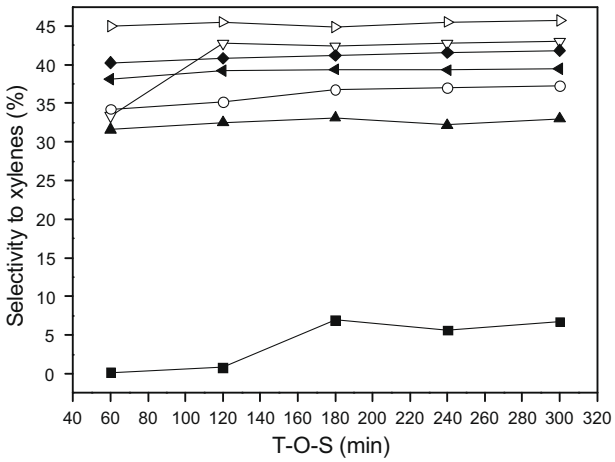

Fig. 7. T-O-S dependence of the selectivity to sum of xylenes in toluene disproportionation over different structural types of zeolites (WHSV – 1.9 h^{-1}, reaction temperature 500 °C). (WHSV – 1.9 h^{-1}, reaction temperature 500 ° C; (◄) BEA, (▽) MCM-68, (▲) SSZ-33, (○) MCM-58, (■) MOR, (▷) ZSM-5, (♦) SSZ-35).

mainly trimethyl or even tetramethyl benzenes and light gases, decreasing the selectivity to xylenes, depends on the void reaction volume in the zeolite channel system and the concentration of acid sites. With increasing reaction volume in the zeolite channels the lowest selectivity to xylenes was achieved over Mordenite, zeolite with the highest concentration of the acid sites. Here, very fast decrease in the toluene conversion was accompanied by the formation of polyalkyl aromatic hydrocarbons (including alkylated napthalenes and anthracenes and light gases, presumably at the expense of xylenes).

Practically no *para*-shape selectivity was observed in toluene disproportionation over any of zeolites studied, using WHSV equal to 1.9 h^{-1}. Under such reaction conditions, even for ZSM-5 *para*/*ortho*-xylene ratio was between 0.98 and 1.03 independent of the T-O-S. The composition of xylene isomers was close to the thermodynamic values for all zeolites under study. When increasing WHSV to 19 h^{-1}, no change in *para*/*ortho*-xylene ratios was observed for other zeolites under study. On the other hand, this ratio over ZSM-5 reached values 1.10 and 1.20 after 15 and 180 min of T-O-S, respectively. It means that with decreasing real contact time, ZSM-5 shifts its behavior to a *para*-selective catalyst.

3.5. Toluene alkylation with isopropyl alcohol

In the case of toluene alkylation with isopropyl alcohol the toluene/isopropyl alcohol molar ratio used in the feed was 9.6, which indicates the theoretical toluene conversion around 10.4% for pure alkylation reaction and complete conversion of isopropyl alcohol. The reaction was carried out at the reaction temperatures of 200 and 250 °C. Literature reports clearly show that toluene conversion depends on the channel diameters of zeolites studied although desorption and transport were proposed as the rate controlling step of the whole alkylation reaction [52]. Selectivity to *p*-isopropyltoluene higher than thermodynamic value (around 30–35%) was achieved only in 10-ring zeolites such as ZSM-5 or ZSM-11. Formation of undesired *n*-propyltoluenes proceeds due to a special channel arrangement in the cross-sections of medium pore channels (ZSM-5) [52] or in zeolite cavities of MCM-58 [50].

3.5.1. The effect of the zeolite structure

Fig. 8A shows the toluene conversion over SSZ-33 after 15 min of T-O-S being 21%, which evidences competition between alkylation and disproportionation. The same can be observed at the reaction temperature of 200 °C, where toluene disproportionation

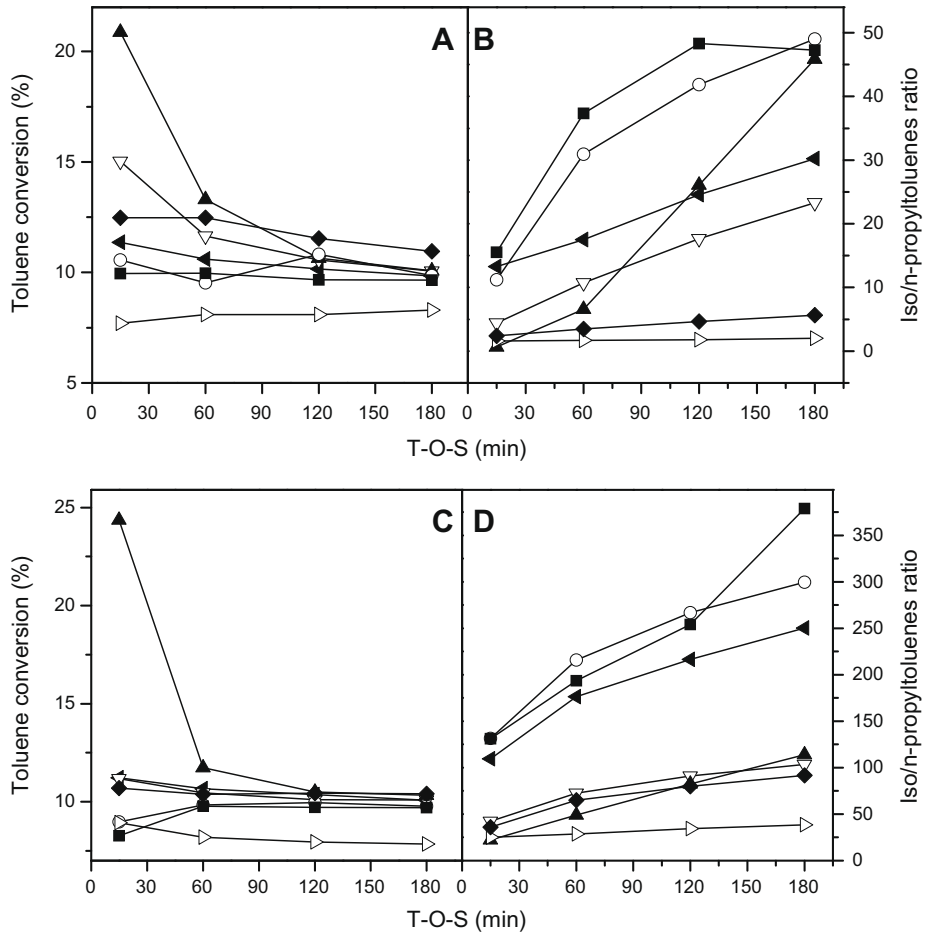

Fig. 8. T-O-S dependence of toluene conversion (A and C) and *iso*-/*n*-propyl toluene ratio (B and D) in toluene alkylation with isopropyl alcohol over different structural types of zeolites (WHSV – 10 h^{-1}, toluene/isopropyl alcohol molar ratio = 9.6, reaction temperature 250 °C (A and B) and 200 °C – (C and D)). ((◄) BEA, (▽) MCM-68, (▲) SSZ-33, (○) MCM-58, (■) MOR, (▷) ZSM-5, (♦) SSZ-35).

is substantially limited over all other zeolites (Fig. 8C). Toluene alkylation proceeds with a high reaction rate over SSZ-33. High value of toluene conversion might be related to the highest acid strength of Brønsted acid sites together with the open structure of this large-pore zeolite. The less open structure of MCM-58 with the same acid strength provides lower toluene conversion. Toluene conversions in toluene alkylation with isopropyl alcohol at 250 °C over different structural types of zeolites decrease at 15 min of T-O-S in the following order SSZ-33 > MCM-68 > SSZ-35 > Beta > MCM-58 > Mordenite > ZSM-5. However, these values are substantially influenced by high rates of toluene disproportionation over zeolites exhibiting strong acid sites and large pore systems. This is particularly seen for SSZ-33 and MCM-68 where at 15 min of T-O-S the selectivities to the sum of propyltoluenes (*iso*-propyltoluenes + *n*-propyltoluenes) are only 3% and 20%, respectively. About 70–75% of toluene converted is transformed into benzene and xylenes via toluene disproportionation. During the first 180 min of T-O-S, toluene conversion over SSZ-33 and MCM-68 decreased to 10–11%, which is mainly due to the deactivation of both zeolites. This conversion decrease is accompanied by a substantial increase in the propyltoluene selectivity, reaching 65–70%. Toluene conversions over zeolites Beta, Mordenite, MCM-58, and SSZ-35 are from 10% to 12%, which is due to a much smaller contribution of toluene disproportionation to the overall toluene conversion. In the case of SSZ-35 and MCM-58 the slow decrease in conversion can be related to the lowest concentration of Lewis acid sites (cf. Table 2). Over these catalysts the increase in the selectivity to *iso*-propyltoluenes is not so steep as for SSZ-33 and MCM-68 as the initial *iso*-propyltoluene selectivity is in the range of 30–50% after 15 min of T-O-S (Fig. 9A). A slight increase in toluene conversion over ZSM-5 zeolite is connected with the fact that desorption and transport of products in toluene alkylation with isopropyl alcohol is the rate-controlling step of this reaction [52]. At 200 °C at 15 min of T-O-S, the order of toluene conversion is as follows: ZSM-5 ~ MCM-58 ~ Mordenite < SSZ-35 ~ Beta ~ MCM-68 < SSZ-33 showing a lower role of channel structure and acidity on the resulting toluene conversion.

3.5.2. The effect of acidity of zeolites

When comparing the concentration of acid sites and their strength with toluene conversion in toluene alkylation with isopropyl alcohol, we can see that due to a high rate of coking substantial changes in conversion order are achieved with 180 min of T-O-S over different zeolites (see Fig. 8A). The highest conversions (due to toluene disproportionation) were observed over SSZ-33 and MCM-68 at 15 min of T-O-S at 250 °C and over SSZ-33 at 200 °C. Relatively high toluene conversions at 250 °C were achieved over SSZ-35 (12.5%) and MCM-58 (10.7%), which are zeolites with intermediate concentration of acid sites and moderate acid strength. The lowest toluene conversion was achieved over ZSM-5 zeolite of the lowest concentration of the acid sites. For T-O-S values longer than 120 min, SSZ-35 dominates in toluene conversion despite a low amount of acid sites and 1-D 10-ring channel system. The highest toluene conversion over SSZ-35 and

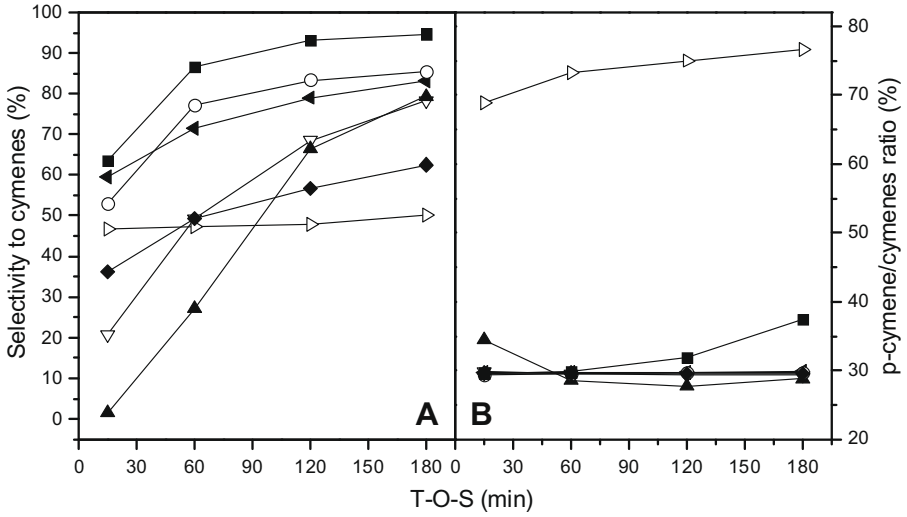

Fig. 9. T-O-S dependence of selectivity to cymenes (A) and selectivity to *p*-cymene in cymenes (B) in toluene alkylation with isopropyl alcohol over different structural types of zeolites (WHSV – 10 h^{-1}, toluene/isopropyl alcohol molar ratio = 9.6, reaction temperature 250 °C). ((◂) BEA, (▽) MCM-68, (▲) SSZ-33, (○) MCM-58, (■) MOR, (▷) ZSM-5, (♦) SSZ-35).

also not pronounced deactivation could be related to a limited formation of bulkier undesired products in the specific channel structure of this zeolite having STF 18-ring cages. As discussed *vide-supra* the acidic properties of zeolites under study provided an order of increasing concentration of Brønsted sites as follows: ZSM-5 < SSZ-35 < SSZ-33 < Beta < MCM-58 < MCM-68 < Mordenite and of all acid sites (Brønsted plus Lewis) as follows: ZSM-5 < SSZ-35 < MCM-58 < SSZ-33 < MCM-68 < Beta < Mordenite (Tables 2 and 3). As the reaction temperature for toluene alkylation is only 250 °C, much more important role of diffusion, which is also related to the concentration of acid sites can be expected. The ease of diffusion was tested by pivalonitrile desorption and the following order was achieved: Beta < MCM-58 < MCM-68 < SSZ-33 < ZSM-5 < SSZ-35 < Mordenite, with Mordenite keeping pivalonitrile the strongest.

A low concentration of acid sites could enhance the rate of diffusion of both reactants and products as shown for ZSM-5 zeolite [33]. Similar behavior can be seen over MCM-58, a 12-ring zeolite with cavities in an undulating 1-D channel system. Deactivation over MCM-58 due to coke formation is rather low and toluene conversion is comparable with 3-D zeolites having 12-ring channels such as Beta, SSZ-33, and MCM-68 (Fig. 8A). Both SSZ-35 and MCM-58 possess strong acid sites, particularly of Lewis type. No clear conclusions can be reached as for the role of acid strength and concentration and channel structure related to toluene conversion in toluene alkylation with isopropyl alcohol over this series of zeolites. Toluene conversion cannot be straightforwardly related either to the concentration of the acid sites or to their acid strength, especially when zeolites with high acid strength contain very low concentrations of active sites and vice versa. The highest toluene conversion at 180 min T-O-S was achieved with SSZ-35 (low concentration of acid sites, medium strength) having a special cage structure, while the lowest was ZSM-5 (the lowest concentration of acid sites). All other zeolites studied despite differences in acidity, size of the channels, and their channel dimensionality exhibited practically the same toluene conversion. However, it will be seen later that the structure played a decisive role for selectivity.

When the alkylation reaction was performed at 200 °C no significant changes in toluene conversions with T-O-S were obtained and all zeolite catalysts exhibited conversions around 10% (Fig. 8C). The only exceptions were ZSM-5 exhibiting toluene conversions around 7% and SSZ-33 (15% at 15 min of T-O-S) due to a fast deactivation caused by toluene disproportionation.

3.5.3. The selectivity to propyltoluenes

The overall concentration of propyltoluenes increases over all zeolites with T-O-S with the exception of ZSM-5. More specifically, while the concentration of *n*-propyltoluenes decreases with T-O-S, the concentration of cymenes exhibits the opposite trend. As for large pore zeolites, the overall concentration of *iso*-propyltoluenes and *n*-propyltoluenes is higher than 80% after 180 min of T-O-S while in the case of Mordenite it reached even 96% under our reaction conditions (Fig. 9). Over MCM-68 and SSZ-33 having open 3-D structures and strong acid sites (mainly of Lewis type) even at 180 min of T-O-S, toluene disproportionation still proceeds with a reasonable rate, the results of which is the selectivity to the sum of benzene and xylenes being between 8 and 10%. Also cumene and ethyltoluenes are formed in consecutive reactions. In contrast, medium pore zeolites SSZ-35 and especially ZSM-5 exhibit a lower decrease in the concentration of *n*-propyltoluenes formed, which is attributed to their channel architecture (vide infra).

For all zeolites under study with exception of ZSM-5, the selectivity to *p*-isopropyl toluene was close to 30% despite the T-O-S values, roughly independent of the T-O-S and close to the thermodynamic value (Fig. 9B). This is connected with the presence of 12-ring channels in zeolites SSZ-33, Mordenite, MCM-58, and MCM -68 and Beta and the presence of 18-ring cavities in 10-ring channels of SSZ-35 decreasing the differences in the rate of transport of individual isopropyl toluene isomers. On the other hand, medium-pore ZSM-5 zeolite behaves as *para*-selective catalyst in toluene alkylation with isopropyl alcohol and its selectivity to *p*-isopropyl toluene reaches almost 80% at 180 min of T-O-S.

In a recent paper of Maekawa and coworkers, the authors studied the effect of corrugation in 1-D channels of zeolites SSZ-55 (ATS topology), SSZ-42 (IFR), and SSZ-35 (STF) on the selectivity in biphenyl alkylation with isopropyl alcohol [53]. It was reported that 12-ring corrugated channels of zeolites SSZ-55 and SSZ-42 did not show any increased selectivity to 4,4′-di-isopropylbiphenyl. No increase in selectivity was observed even in the 10-ring system of corrugated channels of SSZ-35 due to their large size. Based on our investigation, biphenyl should be located parallel to

the channel direction having, most probably, each benzene ring in a different STF cage. In such a location not only 4, 4′ but also positions 2, 2′, 3, and 3′ are accessible for alkylation thus resulting in observed low selectivity to 4,4′-di-isopropylbiphenyl.

3.5.4. Iso-/n-propyltoluene ratio

From the practical point of view the amount of *n*-propyltoluenes formed is critical as for the further application of *iso*-propyltoluenes. With increasing reaction temperature the concentration of *n*-propyltoluenes steadily increases and the *iso*-/*n*-propyptoluene ratio decreases independently of the zeolite catalyst used (cf. Fig. 8B and D). In the last decade it was experimentally evidenced that *n*-propyltoluenes are formed via bimolecular reaction of primary alkylation products, *iso*-propyltoluenes, with toluene being in excess in the reaction mixture [52]. The experimental evidence based on kinetic measurements and NMR studies using labeled compounds [54,55] was also supported by quantum chemical calculations of the reaction mechanism [56]. The proposed reaction mechanism of *n*-propyltoluenes formation is expected to proceed particularly in intersecting medium-pore zeolites such as ZSM-5 and ZSM-11. The importance of proper channel architecture was shown while the acid strength of bridging Si–OH–Al groups enhances the rate of the bimolecular reaction, (Al)ZSM-5 > (Fe)ZSM-5 [57]. Later on, it was shown that also zeolites possessing cages of suitable size such as MCM-58 can provide a proper reaction volume for this bimolecular reaction. On the other hand, the results on MCM-22, where alkylation reaction proceeds preferentially on the outer surface [50] and the concentration of *n*-propyltoluenes formed was rather limited, again point to the need for the exact space, in which the reaction can proceed. Substantial differences in *iso*-/*n*-propyl toluene ratio in the dependence on the structure of the zeolite investigated show that *iso*-/*n*-propyl ratio increases (see Fig. 8B and D)

(i) with increasing size of the channels,
(ii) with increasing connectivity of channels,
(ii) for longer T-O-S values.

The first two factors are typically geometrical while the third one is most probably connected with the deactivation of zeolites due to the blocking of active sites.

A special situation is for zeolites having cages in their 1-D channel structures independently whether the original is a 10-ring or a 12-ring channel as for SSZ-35 and MCM-58, respectively. For experiments performed at 250 °C at 15 min of T-O-S the lowest values of *iso*-/*n*-propyl toluene ratios were reached with SSZ-33 and ZSM-5, followed by SSZ-35 and MCM-68, all being lower than 5 (Fig. 8B). Mordenite, Beta and MCM-58 exhibited *iso*-/*n*-propyl toluene ratios already higher than 5. Much larger differences were found after 180 min of T-O-S. Only 10-ring zeolites ZSM-5 and SSZ-35 exhibited *iso*-/*n*-propyl toluene ratios lower than 6, ZSM-5 = 2.0 while SSZ-35 = 5.7. This is due to the fact that ZSM-5 zeolite structure is close to the optimum one as for the formation of bulky and rather rigid transition state leading to the formation of *n*-propyltoluenes [52]. In the case of zeolite SSZ-35 possessing medium pore channels of similar size as ZSM-5, the most important for the formation of *n*-propyltoluenes seems to be the 18-ring part of the channels. Assuming the location of acid sites (bridging OH groups and Lewis acid sites) close to the channel part coming from 10 to 18 rings we can propose that cymene molecule will be adsorbed in 10 rings having only the possibility of rotation along the C2 axis while another toluene molecule in the 18-ring part of the channel can interact with methyl group to form the bimolecular complex. *Iso*-/*n*-propyl toluene ratio over MCM-68 having 12–10–10-ring system was 23.30, while zeolite Beta having 3D system of 12-ring channels exhibited *iso*-/*n*-propyl toluene ratio equal to 30.3. Although zeolite Beta possesses 3D system of 12-ring channels, one of them is just 5.6–5.6 Å, which is very close to 10-ring channel. The highest *iso*-/*n*-propyltoluene ratios were achieved with Mordenite and MCM-58 both of them are only 1-D channels and SSZ-33. SSZ-33 is 12–12–10-ring zeolite, thus, possesses two large pore channels and one medium pore channel with sizes close to zeolite Beta.

When the alkylation was carried out at the reaction temperature of 200 °C the *iso*-/*n*-propyl toluene ratio was much higher than at 250 °C, which is due to a limited reaction rate of the bimolecular reaction. On the other hand, the increase in the reaction temperature above 250 °C resulted in a further decrease in *iso*-/*n*-propyl toluene ratio as *n*-propyl group is more thermodynamically favored at higher temperatures. Increasing WHSV as well as decreasing toluene/isopropyl alcohol molar ratio resulted in lower *iso*-/*n*-propyl toluene ratio. This is due to the shortening of the real contact time at lower WHSV while decreasing toluene/isopropyl alcohol ratio leads to increasing formation of coke deposits and decreasing the real toluene excess in the reaction mixture. The toluene excess is very important for the rate of the bimolecular reaction as toluene is much less active than *iso*-propyltoluene.

The bimolecular transition state leading to the formation of *n*-propyltoluenes requires again the reaction between toluene and isopropyl toluene molecules in two adjacent cavities with the isopropyl group located close to the center of 10 rings. In such a case, another toluene molecule is allowed to approach the methyl group of the isopropyl group and to form the transition state, as demonstrated by the modeling results (Fig. 5B). The selective formation of *n*-propyltoluenes in the cavities of SSZ-35 zeolite represents another very important feature of this special zeolite structure. Of course, from the application point of view it leads to the formation of undesirable product.

3.6. p-Xylene alkylation with isopropyl alcohol

In *p*-xylene alkylation with isopropyl alcohol at 60 min of T-O-S, SSZ-33, Beta, and SSZ-35 reached *p*-xylene conversions about 70 % with the highest selectivity to 1-isopropyl-2,5-dimethyl-benzene over SSZ-35 (>90%). SSZ-35 also exhibited the highest conversion stability among all zeolites under study (Fig. 10A). To reach the same conversion WHSV of 0.2 h^{-1} were used for all zeolites with the exception of zeolite Beta having a WHSV of 0.5 h^{-1} to compare the catalytic behavior at the same initial conversion level. The dominant catalytic behavior of SSZ-35 over other zeolites in *p*-xylene alkylation is clearly shown in Fig. 10A. The rate of deactivation is lower than over SSZ-33 and Beta. *p*-Xylene conversion over ZSM-5 is only 2–3% compared with more than 70% for SSZ-35, although the concentration of acid sites in ZSM-5 (0.468 mmol g^{-1}) is slightly higher than for SSZ-35 (0.416 mmol g^{-1}), cf. Table 2. In contrast, channel system of ZSM-5 zeolite is too small for the penetration of 1-isopropyl-2,5-dimethyl-benzene molecules even when they are already formed inside the channel system.

The selectivity to 1-isopropyl-2,5-dimethyl-benzene over zeolite Beta (83–80%) was lower than over SSZ-35 (91%) due to the large volume in the channels of zeolite Beta (Fig. 10B), mainly due to the formation of other isomers of isopropyl-dimethyl-benzene, while no *n*-propyl isomers were found. It should be stressed that in *p*-xylene alkylation the first alkylation step leads always to the same product, 1-isopropyl-2,5-dimethyl-benzene and all other products have to be formed by consecutive reactions. It results in two important conclusions: (i) STF cages in SSZ-35 have the suitable size and shape to allow the formation of 1-isopropyl-2,5-dimethyl-benzene, (ii) all other products have to be formed by consecutive reactions. In contrast to zeolites SSZ-33 and Beta, consecutive reactions in SSZ-35 are limited probably more due to a lower acid site concentration in SSZ-35 and not from steric reasons

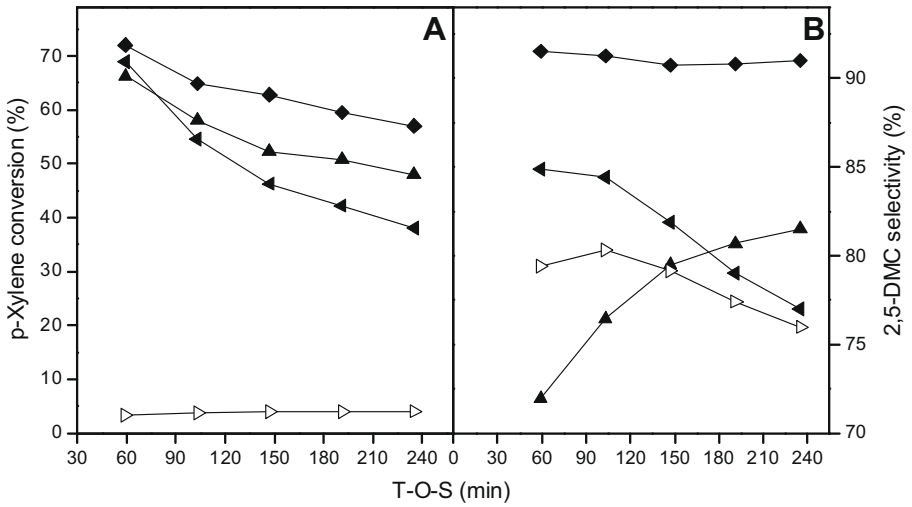

Fig. 10. Time-on-stream dependence of *p*-xylene conversion (A) and selectivity to 1-isopropyl-2,5-dimethyl-benzene (B) in *p*-xylene alkylation with isopropyl alcohol over different zeolites; reaction temperature 150 °C, *p*-xylene/isopropyl alcohol molar ratio = 1:2, WHSV = 0.2 h^{-1} for SSZ-35, ZSM-5, and SSZ-33, and 0.5 h^{-1} for BEA ((◄) BEA, (▲) SSZ-33, (▷) ZSM-5, (♦) SSZ-35).

as at least one of the isomers is of smaller kinetic diameter than 1-isopropyl-2,5-dimethyl-benzene.

Molecular modeling showed that 1-isopropyl-2,5-dimethyl-benzene nicely fits into the 18-ring cavity of SSZ-35 with multiple configurations. As shown in Fig. 5C, its benzene ring is parallel to the channel axis, similar to the configurations that are expected for toluene disproportionation, with both methyl groups being almost perpendicular to the channel axis. The isopropyl group is positioned almost in the center of the 10 rings. The extraordinarily stability of SSZ-35 zeolite in *p*-xylene alkylation benefits from the optimum cavity size for the formation of 1-isopropyl-2,5-dimethyl-benzene and simultaneously prevents the formation of bulkier products due to the *restricted transition state* selectivity [5]. FTIR measurements carried out with pivalonitrile showed that all bridging Si–OH–Al groups are accessible although the kinetic diameter (0.60 nm) of this probe molecule is larger than the size of 10-ring channels (approx. 0.55 nm). The adsorption measurements carried out with *para*- and *meta*-xylenes and 1-isopropyl-2,5-dimethyl-benzene followed by FTIR confirmed an easy accessibility of all acidic sites in SSZ-35 even at ambient temperature. The *p*-xylene conversion over SSZ-35 is one order of magnitude higher than that over ZSM-5 zeolite samples with similar concentration of acid sites and similar crystal size and is comparable with SSZ-33.

4. Conclusions

Seven different structural types of zeolites were investigated in toluene disproportionation as well as alkylation with isopropyl alcohol and *p*-xylene alkylation with isopropyl alcohol to understand the structure/activity/acidity relationship. No straightforward relationship was observed among zeolite activity/selectivity and their acidity and channel architecture. Zeolite activities in alkylation and disproportionation reactions of aromatic hydrocarbons investigated follow neither the order of increasing acidities (both concentration and strength of acid sites) nor the increasing size and connectivity of their channels. These two factors: channel architecture and acidity have to be always considered in parallel.

Generally, toluene and *p*-xylene conversions increase in parallel with increasing concentration and strength of acid sites as well as with increasing size and connectivity of the channels. However, both factors define the stability of zeolites against coking – the higher is the acid site concentration, the higher is the deactivation rate. Similarly, the more open the zeolite channel structure, the faster the deactivation. In such cases, very high initial activity governed by a high number of active centers decreases rapidly. Decrease in the activity is usually connected with increasing shape-selectivity, caused by the blockage of the channels by bulky coke deposit thus, decreasing the reaction volume in the channels.

The opposite trend can be observed for zeolites, containing in their system cages of bigger dimensions than the nominal channel sizes, such as zeolite MCM-58 and SSZ-35. The presence of the cages is 'sheltering' the active sites from coking and at the same time allowing formation of bulky transition-state, therefore placing these zeolites much higher in the activity order than should be expected taking into account only their nominal channel sizes, dimensionality or even acidity. SSZ-35 seems to be the special case, as the cavities of this zeolite are of the sizes of such dimensions that 'fits' the transition-state of the toluene disproportionation reaction. The presence of cages in the 1-D channel systems of zeolites MCM-58 (12-ring) and SSZ-35 (10-ring) shifts their catalytic behavior to "higher" level and both zeolites are rather resistant against deactivation due to a limited formation of carbon residues.

More specifically, the highest toluene conversion in its disproportionation at 500 °C was observed over Mordenite having the highest concentration of both Brønsted and as all acid sites (Brønsted plus Lewis). However, Mordenite deactivates very quickly in contrast to other zeolites studied. For other zeolites (MCM-68, MCM-58, Beta, SSZ-33, and SSZ-35) acid strength seems to be the factor dominating their activities.

The highest stability against deactivation in toluene disproportionation was observed with ZSM-5, MCM-58, and SSZ-35, two of them being 1-D zeolites possessing cages in their structures. Their presence most probably limits the formation of bulky organic deposits while not significantly hindering the transport of reactants and products.

In the case of toluene alkylation with isopropyl alcohol, the initial conversion particularly over SSZ-33 is substantially influenced by the rate of toluene disproportionation at both reaction temperatures (200 and 250 °C). After 180 min of T-O-S the highest toluene conversions were achieved over SSZ-35 and MCM-58, both 1-D zeolites channels having cages along their channels.

Formation of undesired *n*-propyltoluenes is not only limited on medium-pore zeolites with intersecting channels but also *n*-pro-

pyltoluenes can be easily formed in cages of SSZ-35 and even MCM-58.

In addition, we have shown an unusual catalytic behavior of medium pore zeolite SSZ-35, the structure of which combines 10-ring portal openings into shallow 18-ring cavities. This unique feature of the SSZ-35 zeolite is reflected not only in its high activities in different reactions of aromatic hydrocarbons but also in very high resistance toward deactivation. The interplay between 10- and 18-ring sections of the one-dimensional channel system represents a peculiar reaction space for preventing the formation of various bulkier transition states, providing high selectivities to different products. Experimental results are supported by molecular modeling, which confirms the preferred locations of molecules or precursors of transition states in the channel system, leading to the reactions between two molecules located in the neighboring 18-rings through the 10-ring windows. The results demonstrate the very unusual catalytic behavior of medium-pore SSZ-35 zeolite, the catalytic activities of which being higher or comparable with large-pore zeolites, while the selectivities are close to medium-pore zeolites.

Acknowledgments

N.Ž. and J.Č. thank the Academy of Sciences of the Czech Republic for the financial support (1QS400400560). The work of Z.P. was supported by the Grant Agency of the Czech Republic (203/08/H032). IR measurements were supported by the grant from the Ministry of Science and Higher Education, Warsaw, Poland (Project No. N N204 1987 33). The authors also appreciate the support of this work by Chevron.

References

[1] J. Čejka, H. van Bekkum, A. Corma, F. Schűth (Eds), Introduction to Zeolite Science and Practice, third ed., Elsevier, Amsterdam, Stud. Surf. Sci. Catal., vol. 168, 2007.
[2] A. Corma, Chem. Rev. 95 (1995) 559.
[3] P.B. Venuto, Micropor. Mater. 2 (1994) 297.
[4] A. Bhan, E. Inglesia, Acc. Chem. Res. 41 (2008) 559.
[5] J. Čejka, B. Wichterlová, Catal. Rev. 44 (2002) 375.
[6] B. Smit, T.L.M. Maesen, Nature 451 (2008) 671.
[7] B. Wichterlová, J. Čejka, Catal. Lett. 16 (1992) 421.
[8] W.W. Kaeding, G.C. Barile, M.M. Wu, Catal. Rev. – Sci. Eng. 26 (1984) 597.
[9] T. Tsai, S. Liu, I. Wang, Appl. Catal. A 181 (1999) 355.
[10] F.J. Llopis, G. Sastre, A. Corma, J. Catal. 227 (2004) 227.
[11] S. Al-Khattaf, M.A. Ali, A. Al-Almer, Energy Fuels 22 (2008) 243.
[12] S. Rabiu, S. Al-Khattaf, Ind. Eng. Chem. Res. 47 (2008) 39.
[13] S.B. Hong, Catal. Surv. Asia 12 (2008) 131.
[14] S.H. Lee, D.K. Lee, C.H. Shin, Y.K. Park, P.A. Wright, W.M. Lee, S.B. Hong, J. Catal. 215 (2003) 151.
[15] G. Mirth, J. Čejka, J.A. Lercher, J. Catal. 139 (1993) 24.
[16] M.A. Uguina, J.L. Sotelo, D.P. Serrano, Appl. Catal. 76 (1991) 183.
[17] V.P. Shiralkar, P.N. Joshi, M.J. Eapan, B.S. Rao, Zeolites 11 (1991) 511.
[18] S. Melson, F. Schűth, J. Catal. 170 (1997) 46.
[19] M. Bregolato, V. Bolis, C. Busco, P. Ugliengo, S. Bordiga, F. Cavani, N. Ballarini, L. Maselli, S. Passeri, I. Rossetti, L. Forni, J. Catal. 245 (2007) 285.
[20] J.M. Thomas, J. Klinowski, Angew. Chem., Int. Ed. 46 (2007) 7160.
[21] S. Tontisirin, S. Ernst, Angew. Chem., Int. Ed. 46 (2007) 7304.
[22] V.J. Frillette, W.O. Haag, R.M. Lago, J. Catal. 67 (1991) 218.
[23] S.I. Zones, T.V. Harris, Micropor. Mesopor. Mater. 35–36 (2001) 31.
[24] S.I. Zones, C.Y. Chen, A. Corma, M.T. Cheng, C.L. Kibby, I.Y. Chen, A.W. Burton, J. Catal. 250 (2007) 41.
[25] P. Wagner, Y. Nakagawa, G.S. Lee, M.E. Davis, S. Elomari, R.C. Medrud, S.I. Zones, J. Am. Chem. Soc. 122 (2000) 263.
[26] C.Y. Chen, L. W Finger, R.C. Medrud, C.L. Kibby, P.A. Crozier, I.Y. Chan, T.V. Harris, L.W. Beck, S.I. Zones, Chem. Eur. J. 4 (1998) 1312.
[27] D.L. Dorset, S.C. Weston, S.S. Dhingra, J. Phys. Chem. B 11 (2006) 2045.
[28] R.F. Lobo, M. Pan, I. Chan, R.C. Medrud, S.I. Zones, P.A. Crozier, M.E. Davis, J. Phys. Chem. 98 (1994) 12040.
[29] C.Y. Chen, S.I. Zones, Micropor. Mesopor. Mater. 104 (2007) 39.
[30] D.H. Olson, W.O. Haag, ACS Symp. Ser. 248 (1984) 275.
[31] C.W. Jones, S.I. Zones, M.E. Davis, Micropor. Mesopor. Mater. 28 (1999) 471.
[32] J. Čejka, G.A. Kapustin, B. Wichterlová, Appl. Catal. A 108 (1994) 187.
[33] B. Wichterlová, N. Žilková, J. Čejka, Micropor. Mater. 6 (1996) 405.
[34] <http://www.iza-structure.org/databases/>.
[35] S.I. Zones, US Patent 4,963,337, 1990.
[36] Y. Nakagawa, US Patent 5,268,161, 1993.
[37] M. Bejblová, S.I. Zones, J. Čejka, Appl. Catal. A 327 (2007) 255.
[38] G. Košová, Stud. Surf. Sci. Catal. 158 (2005) 59.
[39] Y. Nakagawa, US Patent 5,268,161, 1993.
[40] C.Y. Chen, S.I. Zones, in: A. Galarneau, F. Di Renzo, F. Fajula, J. Vedrine (Eds.), Proc. 13th International Zeolite Conf., Montpellier, France 2001, Elsevier, Stud. Surf. Sci. Catal. 135 (2001) 211.
[41] J. Datka, B. Gil, A. Kubacka, Zeolites 18 (1997) 245.
[42] Cerius2, V. 2.1, Product of MSI and Biosym.
[43] E. de Vos Burchart, Studies on zeolites: molecular mechanics, framework stability and crystal growth, Ph.D. Thesis, 1992 (Table 1, Chapter XII).
[44] A.K. Rappe, C.J. Casewit, K.S. Colwell, W.A. Goddard III, W.M. Skill, J. Am. Chem Soc. 114 (1992) 10024.
[45] G. Paparatto, E. Moretti, G. Leofanti, F. Gatti, J. Catal. 105 (1987) 227.
[46] S. Al-Khattaf, Z. Musilová-Pavlačková, M.A. Ali, J. Čejka, Top. Catal. 52 (2009) 140.
[47] B. Gil, S.I. Zones, S.-J. Hwang, M. Bejblová, J. Čejka, J. Phys. Chem. C 112 (2008) 2997.
[48] E. Brunner, H. Ernst, D. Freude, M. Hunger, C.B. Krause, D. Prager, W. Reschetilowski, W. Schwieger, K.-H. Bergk, Zeolites 9 (1989) 282.
[49] G. Bagnasco, M. Turco, C. Resini, T. Montanari, M. Bevilacqua, G. Busca, J. Catal. 225 (2004) 536.
[50] J. Čejka, A. Krejčí, N. Žilková, J. Kotrla, S. Ernst, A. Weber, Micropor. Mesopor. Mater. 53 (2002) 121.
[51] Y. Xiong, P.G. Rodewald, C.D. Chang, J. Phys. Chem. 117 (1995) 9427.
[52] B. Wichterlová, J. Čejka, J. Catal. 146 (1994) 523.
[53] H. Maekawa, T. Shibata, A. Niimi, C. Asaoka, K. Yamasaki, H. Naiki, K. Komura, Y. Kubota, Y. Sugi, J.-Y. Lee, J.-H. Kim, G. Seo, J. Mol. Catal. A 279 (2008) 27.
[54] I.I. Ivanova, D. Brunel, G. Daelen, J.B. Nagy, E.G. Derouane, Stud. Surf. Sci. Catal. 78 (1993) 587.
[55] I.I. Ivanova, D. Brunel, J.B. Nagy, E.G. Derouane, J. Mol. Catal. A 95 (1995) 243.
[56] J.E. Šponer, J. Šponer, J. Čejka, B. Wichterlová, J. Phys. Chem. B 102 (1998) 7169.
[57] J. Čejka, A. Vondrová, B. Wichterlová, G. Vorbeck, R. Fricke, Zeolites 14 (1994) 147.